Micromachined Electromagnetic Bandgap Crystals as Antenna Substrates for a 500 GHz Imaging Array

L. Azcona, B. Alderman, D. N. Matheson & P. G. Huggard
Rutherford Appleton Laboratory, Chilton, Didcot, OX11 0QX, United Kingdom

B. Martinez, I. Ederra, C. Del Rio & R. Gonzalo
Electrical and Electronic Engineering Department, Universidad Pública de Navarra, Campus Arrosadía, E-31006, Pamplona, Navarra, Spain

B. de Hon & M. C. van Beurden
Faculty of Electrical Engineering, Eindhoven University of Technology, PO Box 513, 5600 MB Eindhoven, The Netherlands

L. Marchand & P. de Maagt
Electromagnetics Division, European Space Research and Technology Centre, PE Box 299, 2201 AG Noordwijk, The Netherlands.

ABSTRACT – **This paper presents the development of a prototype imaging array, operating in a frequency band centred on 500 GHz, which is intended for eventual space deployment. The use of novel Electromagnetic Bandgap (EBG) substrates for the planar antennas of the array offers significant advantages in terms of overall mass, size and antenna directivity. The main emphasis of this paper is on the specialised precision processing techniques required for their realisation.**

The use of high dielectric constant, ε_r, materials yields EBG crystals with wider fractional stopbands and smaller physical dimensions. Consequently, high resistivity silicon, $\varepsilon_r \approx 12$, and ceramic microwave dielectrics, $\varepsilon_r \approx 40$, are used to form the crystals. Three different 3-D EBG designs have been analysed comprehensively and the acceptable dimensional tolerances for each design, as a function of ε_r of the constitutive dielectric material, have been specified.

Characteristic structural dimensions are around 100 µm for 500 GHz EBG crystals. Several different fabrication processes have been considered, the selection being governed by material constraints and dimensional tolerances. For silicon processing, the advantages of deep reactive ion etching over the previously used abrasive sawing method are described. For ceramic materials, the range of processing techniques is limited due to the material characteristics, structure sizes and tight dimensional tolerances required. Laser ablation, abrasive sawing and the use of micron sized abrasive particles in a high velocity air stream are compared.

I. INTRODUCTION

The realisation of imaging arrays for the millimetre wavelength range is of great interest for astronomy and atmospheric research. Up to now waveguide-based technology has been used for these purposes since this provides natural isolation between adjacent pixels. However, the restrictive costs and bulky nature of this approach limits the maximum number of pixels in an array.

The emergence of planar arrays defined by lithography offers the potential realisation of a much larger number of pixels. Nevertheless, the performance of planar antennas can be severely limited by cross coupling through surface waves [1]. Three-dimensional Electromagnetic Bandgap (3D-EBG) structures are designed to suppress the propagation of radiation in a certain frequency range. Thus, using a 3D-EBG as an antenna substrate should attenuate or even eliminate the coupling between array elements via surface waves thereby improving antenna performance. *Figure 1* shows one possible configuration of such an array.

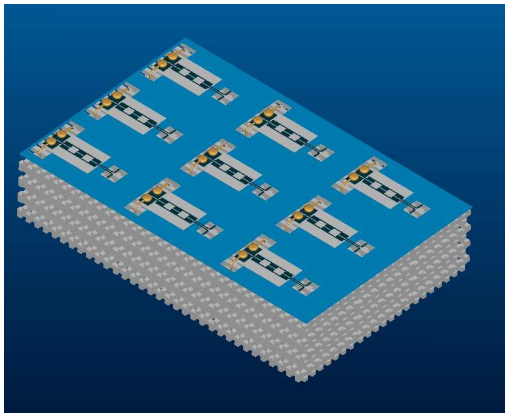

Figure 1: Artist's impression of an array of dipoles on a woodpile Electromagnetic Bandgap Structure.

The frequency range over which the radiation cannot propagate inside a 3D-EBG structure is called the bandgap. The bandwidth and position of the bandgap are given by the band diagram of the EBG structure, *Figure 2*, which plots the relationship between frequency

and wavevectors, k, of the different modes for all directions in the Brillouin zone. The Brillouin zone in turn is determined by the unit cell of the structure [2].

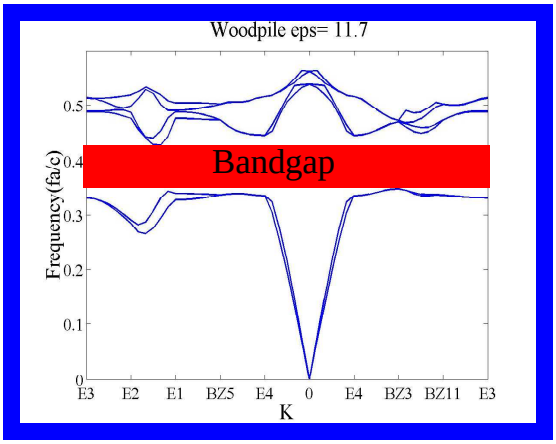

Figure 2: Dispersion relation for the 3D-EBG woodpile structure.

II. MODELLING AND DESIGN

Electromagnetic Bandgap structures are characterised by the range of frequencies where the structure does not permit the propagation of radiation. In a good design this stopband, or bandgap, may have a theoretical fractional width of over 30 % in a material with a high dielectric constant. Several software tools are available for the analysis and design of 3D-EBG structures. Three different methods have been used in the course of this project and they are described in turn below.

The Plane Wave Method (MIT, [3, 4])

The band diagram of a 3D-EBG crystal can be found by a plane wave method. The resulting diagram displays the eigenmodes of the structure, which are the electromagnetic waves that can propagate through the structure for a definite frequency, ω, for various directions indicated by wavevectors, k.

The initial equation to be solved is:

$$\nabla \times \left[\eta(r) \cdot \nabla \times \vec{H} \right] = -\frac{1}{c^2} \frac{\partial^2 \vec{H}}{\partial t^2}$$

The code takes a propagation wavevector and expands the magnetic field in a plane wave basis using Bloch's theorem for periodic media. Working with this equation an eigensystem is found, whose eigenvalues are the frequencies of the dispersion diagram.

Transverse spectrum contrast-source formulation method

Developed by the Faculty of Electrical Engineering of the Eindhoven University of Technology [5], this approach is based on an integro-differential equation for the electric field. It employs a two-dimensional plane-wave expansion in the transverse plane (x-y) and a uniform mesh in the longitudinal direction (z). In the resulting numerical scheme, the computational complexity is dominated by Fast Fourier transformations, which yield an efficient matrix-vector product. The resulting equation is then solved by means of an iterative technique.

Transmission and Reflection Calculations.

Several commercial software tools are available for predicting the transmission and reflection of 3D-EBG structures, and from these Ansoft and HP-HFSS have been selected. These techniques are both based on the finite element method [6].

In practice, the plane wave method and the transverse spectrum contrast-source formulation method are used to calculate the band diagram and consequently the bandgap of the structures. We have found good agreement between the results of the two methods: *Figure 3.*

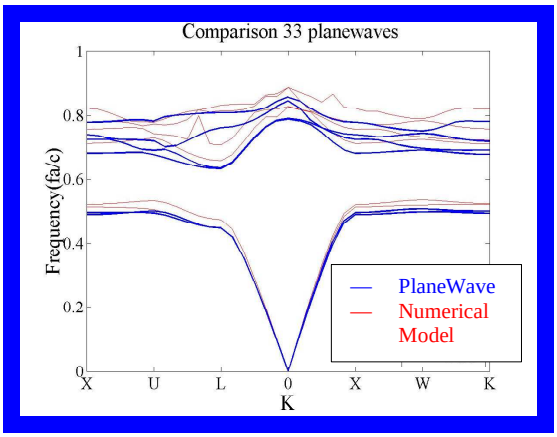

Figure 3: Band diagram comparison for the so-called MIT2 EBG structure – described in text below. The models used 33 plane waves to solve the eigensystem.

Using the three software tools several 3D-EBG structures were analysed and optimised. They are the Woodpile, the MIT1 and the MIT2 structures.

- **Woodpile structure**

This structure was proposed at about the same time by the Iowa State University Group and J.P. Dowling in 1994 [7, 8]. The basis of the structure consists of 4 layers of square dielectric rods having a centre to centre separation *a* as shown in *Figure 4*. The rods are rotated by 90º in each successive layer and displaced by an offset of *a/2* between every second layer.

By optimising the different dimensions of the structure a fractional bandwidth of 21 % is achievable using a material with a relative permittivity $\varepsilon_r = 12$, and a bandwidth of 33 % and 35 % for a material of $\varepsilon_r = 40$ and $\varepsilon_r = 90$ respectively. This centre frequency of the stopband is scalable to any desired frequency by adjusting the structure dimensions and in this case is set at 500 GHz. At this frequency the period, *a*, is 240, 150

and 100 μm approximately for materials of relative permittivity of 12, 40 and 90 respectively.

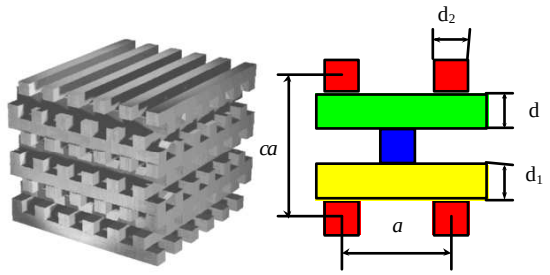

Figure 4: Woodpile structure model and layout.

- **MIT1 structure**

This 3D-EBG structure was proposed in 1994 by MIT group [9]. It consists of two different dielectric materials. Staggered channels of the lower-dielectric material - air in this case - pass through the high-dielectric substrate, and a triangular lattice of air holes is etched through perpendicular to the channels: *Figure 5*.

Optimising the different dimensions of the structure bandwidths of 22 %, 36 % and 38 % are achievable using materials with ε_r of 12, 40 and 90 respectively. At the centre frequency of the design, 500 GHz, the dimensions of the structure are given by a = 400, 250 and 170 μm as ε_r ranges from 12 to 90.

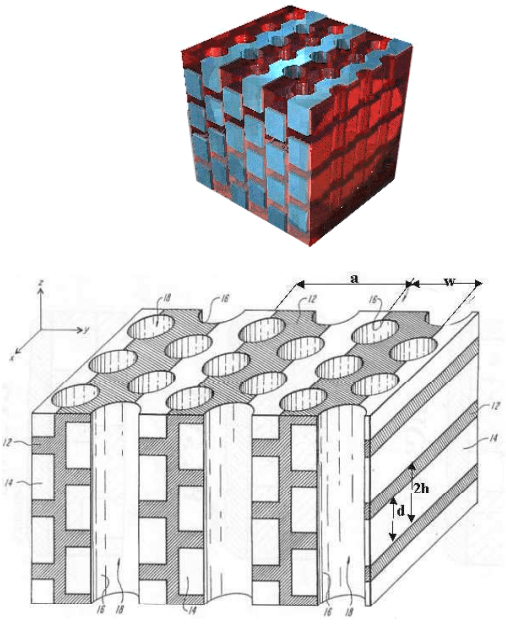

Figure 5: MIT1 Structure model (top) and layout (bottom).

- **MIT2 structure**

This structure has been more recently proposed by MIT [10]. The unit cell is formed by six layers of a shifted stacking of the two characteristic types of 2D-EBG crystals: hexagonal dielectric rods in air and circular air holes in dielectric: *Figure 6*.

Our calculations show that the bandwidths achievable by optimising the different dimensions of the structure are 22 %, 36 % and 38 % for ε_r = 12, 40 and 90 respectively. At the centre frequency of the design, 500 GHz, the dimensions of the structure are defined by the parameter a equal to 450, 300 and 180 μm respectively.

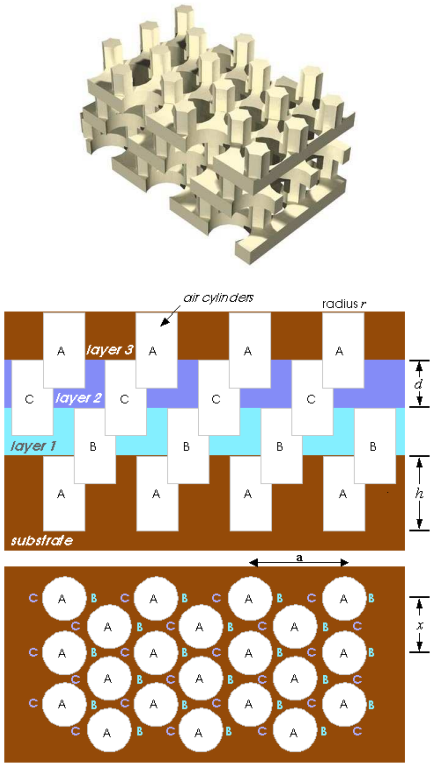

Figure 6: MIT2 structure model (top) and layout (bottom).

All three structures were optimised using the different software tools over the range $12 < \varepsilon_r < 90$. It was found that increasing the relative permittivity leads firstly to smaller structure dimensions and, more importantly, to a wider fractional bandgap.

We found that the bandwidth increases only slightly as ε_r is raised from 40 to 90. On the other hand, the characteristic dimension a decreases and the machining properties of high ε_r ceramic worsen with increasing ε_r. As a consequence, it was decided to use ε_r = 12 and 40 dielectrics for the 3D-EBG crystals.

Two different materials were selected for making the structures:

- High resistivity (> 1 kΩcm) double sided polished silicon wafers, ε_r = 12, (100) orientation with flatness tolerances of ± 4μm.
- D36 ceramic from Morgan Electroceramics, a Zr/Sn Titanate (ZTT) with ε_r = 37.

The sensitivity of the electromagnetic properties of the different structures to small changes in dimensions was also analysed for both materials. Changing the

structure dimensions away from the ideal values leads to a shift in the bandgap centre frequency and to a decrease in bandwidth. Thus, any fabrication process must deliver a dimensional precision that does not result in significant changes in these electromagnetic properties. The objective of this part of the study was to quantify the required manufacturing precision in advance of production.

The electromagnetic properties of both MIT1 and MIT2 structures are most sensitive to variations in the radii of the holes, *Figure 5* and *6*, whereas variations in the bar widths of the woodpile need to be minimised: *Figure 4*. From our analysis, fabrication tolerances should be below ± 5 μm for silicon and ± 2 μm for the ceramic. These tolerances guarantee bandwidths bigger than 20% for the silicon structures and 32% for the ceramic ones. Besides, the tolerances also guarantee a centre frequency variation below ±20 GHz for the silicon case and ±50 GHz for the ceramic case (with respect to a centre frequency of 500 GHz). As expected, the tolerances decrease with increasing ε_r. This is consistent with the decreasing structure size with increasing ε_r.

As an example, the variations in central frequency and fractional bandwidth with respect to bar width are shown in *Figure 7* for the silicon woodpile.

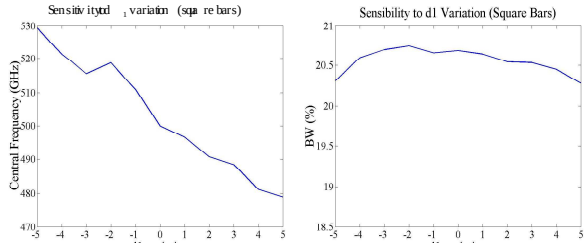

Figure 7: Sensitivity of the central frequency (left) and the fractional bandwidth (right) with respect to the variations in bar width d1 up to ± 5 μm for the silicon woodpile.

III. FABRICATION

Once the structure designs were optimized, the next step was to find micromachining techniques capable of delivering the dimensions and fabrication tolerances required. Several techniques were considered and subsequently rejected as not being able to match the requirements of the application.

This is the case of photolithography where the structures are defined using the ultra-thick resist SU-8. Unfortunately this is very lossy at 500 GHz, the central frequency of the design. The same reason excludes rapid prototyping techniques, such as stereolithography or sintering. Both injection moulding (precision shaping of polymeric materials) [11] and ultrasonic machining were rejected for not being able to achieve the small size of the structures. Mechanical milling, despite being suitable for some ceramics and polymers, does not match the fabrication tolerances as the achievable surface roughness is of order 20 μm. Mechanical drilling was also considered. The consulted company, Agate Products, who specialise in processing sapphire, quartz and another hard substances, advised that the minimum wall thickness between holes should be at least the thickness of the material. This is not the case in the MIT1 and MIT2 structures shown above.

The woodpile structure on silicon has been previously been fabricated using a narrow bladed diamond saw [12]. The process consists of dicing the rods on silicon wafers that are twice the thickness of one layer of the structure, inverting the wafer, and dicing the second layer at 90° to the first. Two different kinds of tiles are defined in this way, with an offset between each other of half the period "*a*" of the woodpile structure (*Figure 4*). The tiles are alternatively stacked using the corners for alignment. This process is described in *Figure 8*.

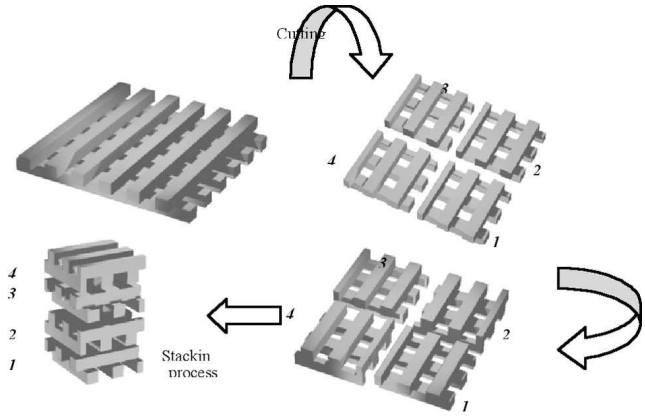

Figure 8: Forming a square bar woodpile by double sided processing of dielectric wafers and then stacking the resulting rectangular tiles.

However, this technique is limited by the surface roughness achievable with the dicing blades, 2 μm approximately. A major weakness of dicing is that only blind and through grooves can be cut by this method, excluding the formation of isolated arbitrary shapes.

Deep Reactive Ion Etching (DRIE) or dry etching of silicon provides a surface roughness of less than 2 μm and the defined pattern accuracy is better than 1 μm. However, this high etch rate process is only suitable for the forming of silicon, for maximum practical etch depths in other materials are only a few microns. DRIE was selected for defining the silicon woodpile structure in preference to dicing. The pattern to be etched was first written, using a silicon dioxide mask, on both surfaces of 140 μm thick silicon wafers. The wafers were etched from one surface to a depth of 70 μm. They were turned over and etched again to the same depth, thus defining a tile with two layers of the woodpile structure. Again, two different tiles had to be manufactured. Through dowel holes and 70 μm deep ball holes [13] were also etched to allow accurate stacking: *Figure 9*.

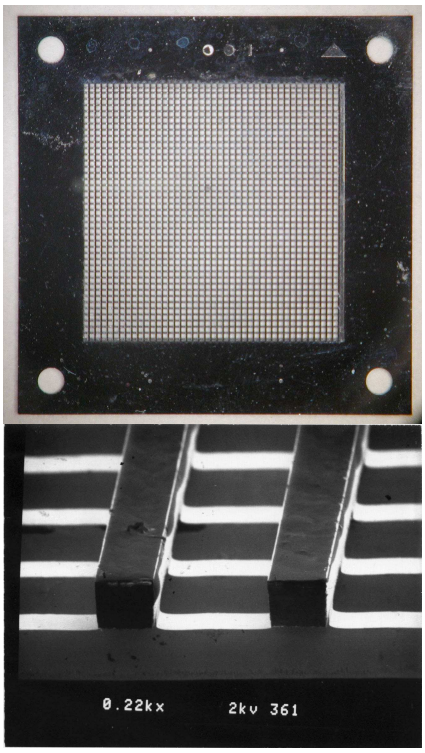

Figure 9: Double-side etched silicon tile (top) and closer view of the processed silicon wafer (bottom). Wafer thickness 140 μm. Bars width and depth 70 μm. Centre to centre distance between bars is 230 μm.

The MIT1 structure can be defined by stacking layers in either vertical or horizontal planes since it is periodic in both directions (*Figure 5*). Instead of using two solid dielectrics of low and high relative permittivity, air filled spaces form the low permittivity dielectric, resulting in a higher contrast and better performance [2]. If horizontal layers are chosen to define the structure, parallel bars may be diced in tiles that have been previously drilled with an array of holes. However, if the layers are chosen to be vertical, both the rods and the holes can be diced if the blade profile produces a semicircular cut: *Figure 10*. It is important to point out that by using horizontal layers it is possible to build the structure with only one kind of tiles, whereas in the case of vertical stacking, two kind of tiles are needed.

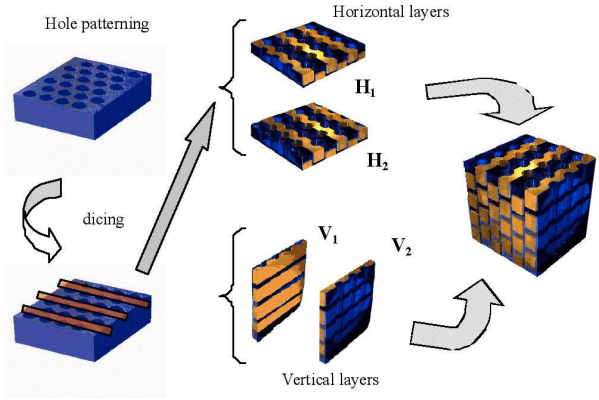

Figure 10: MIT1 fabrication process: hole patterning by laser ablation or grit blasting, defining rows by high precision diamond sawing and stacking. Fabrication methods are described in the text.

On the other hand, the MIT2 structure can only be formed by horizontally stacking identical layers of hexagonal pillars and holes. Three such tiles, stacked with different offsets, are needed to define one period of the structure in the z-direction (*Figure 6*). The planned method is similar to the one selected for the MIT1 structure and consists of dicing the hexagonal pillars on previously drilled tiles. *Figure 11* describes the process.

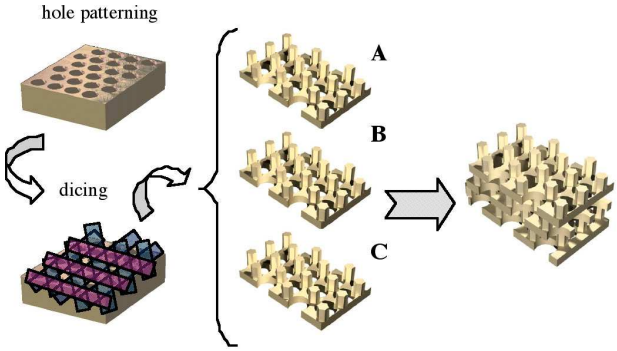

Figure 11: MIT2 defining process. Three tiles are needed for one period of the structure (Figure 6).

For the MIT1 structure, high precision diamond sawing has been selected to define the channels. In case that vertical stacking is selected, both the channels and the holes may be defined by respectively using rectangular and semicircular blade profiles. The same method will be used to define the hexagonal pillars of the MIT2 structure.

An automated Disco DAD321 dicing saw with a three-axis step precision of 0.2 μm [14] has been used to make several tests. Results from silicon, shown in *Figure 12*, are excellent. Some improvements are still needed in processing the ZTT ceramic although the initial results are very promising. The profiles produced in the ceramic have rounded internal corners, *Figure 13*, so special blades have been ordered to obtain the desired near perpendicular corners.

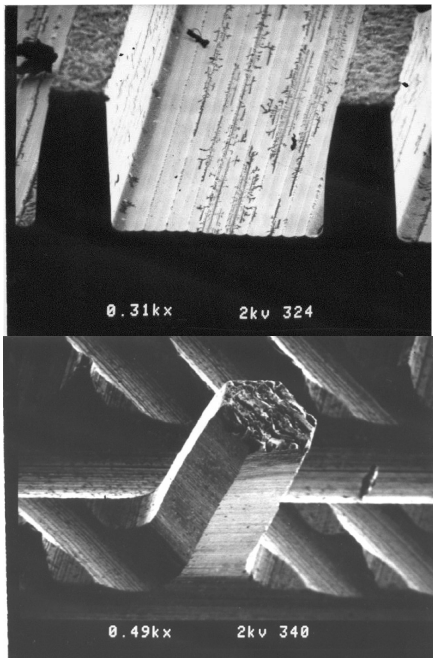

Figure 12: 70 µm wide, 135 µm high MIT1 pillars, gap between rows 190 µm, (top) and 130 µm high, 36 µm side MIT2 hexagonal pillar (bottom) diced in silicon using high precision diamond sawing.

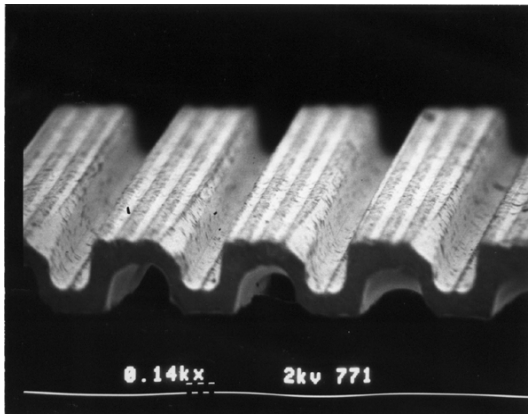

Figure 13: 165 *µm thick ZTT sample cut with the dicing saw. This has 90 µm deep and 90 µm wide cuts, wall thickness 30 µm.*

Prior to dicing the channels and pillars of the actual MIT structures, the hexagonal lattice of holes will be defined using either laser ablation or grit blasting, as described below

Laser ablation is achieved by focussing a high power pulsed laser onto the sample, breaking atomic bonds and converting the material into plasma. This technique is suitable for ceramics and is capable of delivering a surface roughness below ± 3 µm. A triangular lattice of similar dimensions to the actual MIT1 and MIT2 structures was successfully patterned in an 80 µm thick ZTT sample, *Figure 14*, using X-Y stepped UV laser pulses [15].

Grit blasting is based on a high velocity stream of air that carries graded particles of abrasive which mechanically remove some of the dielectric upon impact. A mask, which resists abrasion, is needed to define the structure. The technique is suitable for both silicon and ceramics and it should be capable of achieving a hole aspect ratio of 1:2.5 and with a surface roughness better than ± 2 µm.

Whereas laser ablation has proven to be successful in several tests on ceramic, grit blasting is a new technique. Although previous studies look very promising [16, 17] the real capabilities of the technique have yet to be realised. For this reason we believe that laser ablation is the approach of choice for producing the required hole arrays.

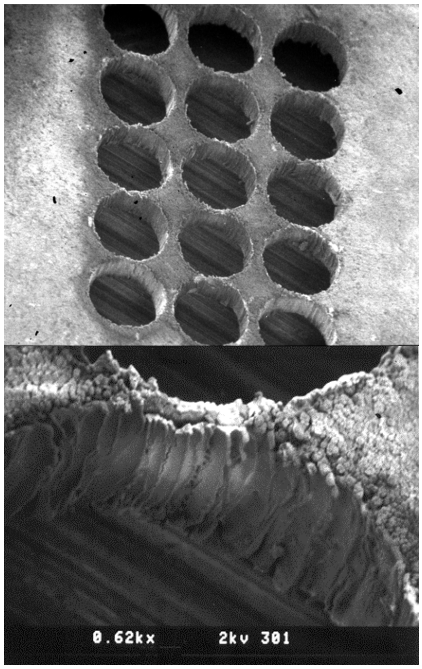

Figure 14: *Laser ablated holes in 80 µm thick ceramic, hole diameter: 200 µm, minimum separation: 15µm*

IV. CONCLUSIONS

The design of several EBG structures suitable for use as substrates for a 500 GHz imaging array have been presented. These EBG structures have been analysed and optimised using different software tools: the results of commercial products (Ansoft & HP HFSS) and in-house designed software were in good agreement. The best EBG structures were found to have a calculated bandgap of 36 % for $\varepsilon_r = 40$ ceramic. Higher permittivity dielectrics deliver a better electromagnetic performance but microfabrication requirements become more demanding: the structures have smaller characteristic dimensions and the materials are harder and more brittle.

Maximum acceptable changes in the bandwidth and central bandgap frequency of the different structures determine the manufacturing tolerances in each case.

These were calculated as ± 5 µm using silicon as the dielectric and ± 2 µm for the ZTT ceramic.

Several fabrication techniques have been presented, and their capabilities and limitations have been discussed. Fabrication tests have been carried out using high precision diamond dicing sawing and laser ablation. A silicon woodpile structure has been successful fabricated using DRIE.

V. REFERENCES

1 - R. Garg, P. Bhartia, I. Bahl and A. Ittipiboon "*Microstrip Antenna Handbook*", Artech House (2001)

2 - J. D. Joannopoulos, R. D. Meade, J. N. Kinn "*Photonic Crystals: Molding the Flow of Light*" Princeton University Press (1995)

3 - S. G. Johnson and J. D. Joannopoulos, "*MIT Photonic-Bands* " http://ab-initon.mit.edu/mpb/

4 - S. G. Johnson and J. D. Joannopoulos, "*Block-iterative-frequency-domain methods for Maxwell's equations in a planewave basis*", Optics Express **8**, 173 (2001).

5 - M.C. van Beurden and B.P. de Hon: "*Electromagnetic modelling of antennas mounted on a band-gap slab -- discretization issues and domain and boundary integral equations*", Int. Conf. on Electromagnetics in Advanced Applications (ICEAA 03), 8-12 September 2003, Politecnico di Torino, Torino Italy.

6 - Ansoft: www.ansoft.com/products/hf/hfss/

7 - K. M. Ho, C. T. Chan, C. M. Soukoulis, R. Biswas and M. Sigalas, "*Photonic bandgaps in three dimensions: New layer-by-layer periodic structure*", Solid State Comm. **89**, 413 (1994).

8 - H. S. Sozuer and J. P. Dowling, "*Photonic band calculations for woodpile structure*", J. Mod. Opt. **41**, 231, 1994.

9 - S. Fan, P. R. Villeneuve, R. D. Meade, and J. D. Joannopoulos "*Design of three-dimensional photonic crystals at submicron lengthscales"* Appl. Phys. Lett. **65**, 1466 (1994).

10 - S. G. Johnson and J. D. Joannopoulos, "*Three-dimensionally periodic dielectric layered structure with omnidirectional photonic band gap"* Appl. Phys. Lett. **77**, 3490 (2000).

11 - Withersdale Plastics Ltd: ww.withersd.demon.co.uk

12 - R. Gonzalo, P. de Maagt, M. Sorolla, "*Enhanced Patch-Antenna Performance by Suppressing Surface Waves Using Photonic-Bandgap Substrates*", IEEE Trans. Microwave Theory Tech. **47**, 2131 (1999).

13 - K. Aoki, H. T. Miyazaki, H. Hirayama, K. Inoshita, T. Baba, N. Shinya and Y. Aoyagi, "*Three-dimensional photonic crystals for optical wavelengths assebled by micromanipulation*", Appl. Phys. Lett. **81**, 3122 (2002)

14 - Disco Corporation: www.disco.co.jp/

15 - Oxford Lasers: www.oxfordlasers.com

16 - Hendrik Wensink, Ph.D. thesis :"*Fabrication of Microstructures by Powder Blasting*", University of Twente, The Netherlands.(2002)

17 - Peter Jan Slikkerveer, PhD thesis: "*Mechanical Etching of Glass by Powder Blasting"*, Philips Electronics N.V. , The Netherlands (1999).